

Study on the Generation of Vortex Waves Based on Coding Metasurfaces and Genetic Algorithms

Shiqi LV¹, Xiangyu CAO², Jun GAO², Rongzhen XUE¹

¹The troops of 94758, Shuimen Village 168 Box Ningde Fujian, 355100, China

²Information and Navigation College, Air Force Engineering University, Fenghao Road 1st Xi'an Shaanxi, 710077, China

2736375493@qq.com, xiangyucaokdy@163.com, gjgj9694@163.com, swol@qq.com

Submitted February 15, 2023 / Accepted May 14, 2023 / Online first June 26, 2023

Abstract. *In this paper, the mechanism of vortex electromagnetic wave generated by coding metasurface is studied, and the shortcomings of this method found through this research, what is more, the reasons for its production are analyzed and summarized. The genetic algorithm is proposed to optimize the arrangement of the encoded metasurface, to improve the angle convergence between the main lobes of the vortex electromagnetic wave, which is conducive to the next transmission detection work. In order to verify this method, two units with phase difference of 180° are designed, and the vortex electromagnetic wave with orbital angular momentum of 1 produced. Finally, the fabricated sample is measured, and the results are in good agreement with the simulation results.*

Keywords

Vortex electromagnetic wave, coded metasurface, genetic algorithm

1. Introduction

With the rapid development of wireless communication technologies for information exchange, the popularity of mobile terminals has gradually increased, and the mobile Internet has shown an explosive development trend. In order to meet the growing demand for mobile data services, there is an urgent need for a new generation of wireless mobile communication technology with higher speed, the MIMO system has received widespread attention [1–3]. Among them, orbital angular momentum technology has become a research hotspot in wireless communication as a multiplexing technology [4].

Orbital angular momentum (OAM) was first discovered in beams in 1992 [5]. Since then, the vortex electromagnetic wave carrying OAM has been widely concerned [6–10]. In the initial study, OAM was mainly concentrated in the field of optics. Since 2007, the concept of OAM was extended to the microwave band and simulated,

using phased array antennas to generate OAM vortex beams [11]. Since then, other techniques such as spiral phase plate (SPP) [12], hologram [13], and circular traveling wave antenna [14] have also been applied to generate OAM vortices in the radio band.

In recent years, the electromagnetic metasurface's powerful ability to regulate electromagnetic waves has attracted more and more people's attention [9], [15–19]. In view of this, a new method for generating OAM vortex radio beams using electromagnetic metasurface is proposed [20]. By adjusting the phase distribution of the metasurface unit, phase adjustment of the incident wave produces a corresponding vortex electromagnetic wave, and is combined with other properties of the electromagnetic wave to regulate [21–23]. However, the design difficulty is too large because the unit control phase should reach 2π and the feed incidence should be considered to maintain the performance of the unit at a large incident angle. In 2018, Zhang Di proposed using a 1-bit metasurface to generate vortex electromagnetic waves, which reduced the difficulty of unit design [24]. However, there are still problems that cannot be ignored in the research. With the increase of the orbital angular momentum, the vortex electromagnetic wave generated by the 1-bit unit has more clutter and the distance between the two main lobes increases, which will undoubtedly increase the difficulty of detection. Conducive to the further transmission of vortex waves.

In this paper, the problems of coding metasurface are analyzed in depth. And the genetic algorithm is used to optimize the arrangement of cells to improve the performance of vortex electromagnetic waves. Firstly, the reason for generating eddy electromagnetic wave clutter on the metasurface is analyzed. The genetic algorithm is used to optimize the unit arrangement, at the same time, the distance between the two main lobes is reduced, and the energy is concentrated on the required vortex wave. Then, a transmissive metasurface was designed and simulated, fabricated and measured experimentally to verify the validity of the numerical calculation. Finally, the work of this paper is summarized.

2. Coded Metasurface Analysis

2.1 Coded Metasurface Vortex Wave Generation Principle

In Fig. 1, a schematic diagram of the transmission of the metasurface vortex wave of the double-layer medium transmission is shown, and Figure 1(b) is a schematic diagram of the vortex wave generated by the metasurface of the feed wave incident transmission type. \mathbf{u}_0 is the transmitted wave direction vector, \mathbf{r}_{mn} is the position vector at point (m, n) , r_f is the vertical distance from the feed to the surface, \mathbf{r}_0 is the wire vector pointed to by the feed point (m, n) , ϕ_{mn} is the angle between \mathbf{r}_{mn} and the y axis, θ is the angle between \mathbf{r}_0 and the z axis.

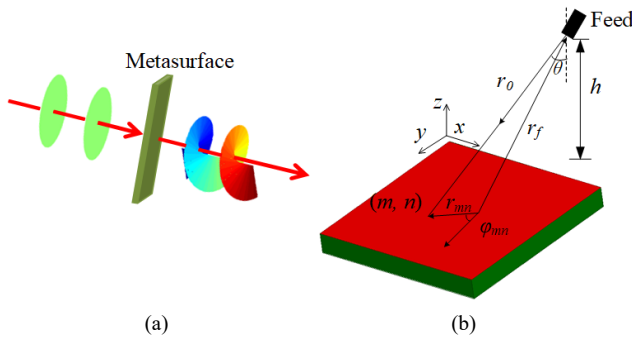


Fig. 1. The schematic diagram of vortex wave generated by transmission-type metasurface: (a) The diagram of vortex wave generation of transmission metasurface with double-layer; (b) The schematic diagram of vortex wave generated by feed-source wave transmission metasurface.

As can be seen from Fig. 1, with $|\mathbf{r}_{mn}|$ increasing, the unit is far from the center of the surface. It is difficult that when the incident wave is the feed wave, the unit needs to maintain good unit characteristics, that is the phase difference and transmittance at different incident angle remain stable. In order to reduce the design difficulty, this paper proposes to use the coded metasurface to reduce the phase control requirements of $0\sim 360^\circ$. The metasurface unit phase distribution can be obtained by (1), M and N are the numbers of units in the x -direction and y -direction of the metasurface, F is the feed function, and A is the metasurface function. After simplification, we can get (2). ϕ_{mn} is the phase required at (m, n) , and l is the orbital angular momentum, and ϕ_{mn}^c can be obtained from (3) and the 360° phase control is discretized into k parts, and the value of j can be obtained ($0 \leq j \leq k$).

$$T(\mathbf{u}) = \sum_{m=1}^M \sum_{n=1}^N F(\mathbf{r}_{mn} \cdot \mathbf{r}_f) A(\mathbf{r}_{mn} \cdot \mathbf{u}_0) A(\mathbf{u}_0 \cdot \mathbf{u}) \cdot \exp\left\{jk_0 \left[|\mathbf{r}_{mn} - \mathbf{r}_f| + \mathbf{r}_{mn} \cdot \mathbf{u}\right] + j\phi_{mn}^c\right\}, \quad (1)$$

$$k_0 \left[|\mathbf{r}_{mn} - \mathbf{r}_f| + \mathbf{r}_{mn} \cdot \mathbf{u}\right] + \phi_{mn}^c = l\phi_{mn}, \quad (2)$$

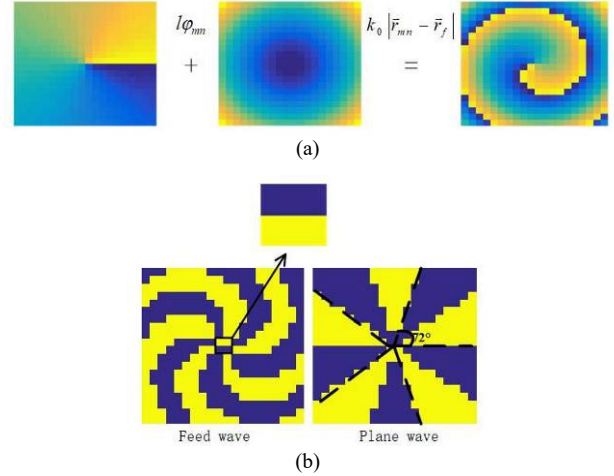


Fig. 2. (a) The diagram of the formula: $k_0 \left[|\mathbf{r}_{mn} - \mathbf{r}_f| + \mathbf{r}_{mn} \cdot \mathbf{u}\right] + \phi_{mn}^c = l\phi_{mn}$. (b) The compensating phase distribution when the vortex electromagnetic wave of $l=3$ is generated by the feed wave into the metasurface.

$$\phi_{mn}^{c*} = \begin{cases} 0^\circ, & -\frac{360^\circ}{2k} \leq \phi_{mn}^c \leq \frac{360^\circ}{2k} \\ \frac{360^\circ}{k} j, & \frac{360^\circ}{k} j - \frac{360^\circ}{2k} \leq \phi_{mn}^c \leq \frac{360^\circ}{k} j + \frac{360^\circ}{2k} \\ 360^\circ, & 360^\circ - \frac{360^\circ}{2k} \leq \phi_{mn}^c \leq 360^\circ + \frac{360^\circ}{2k} \end{cases} \quad (3)$$

Figure 2(a) illustrates the principle that the feed incidence is quasi-continuous (Q-C, a sufficiently large surface, a sufficient number of cells, and a high degree of compensating phase continuity). The metasurface provides a principle for compensating the phase-generated vortex wave, as can be seen from the compensation phase that needs to be provided when the feed incident on the metasurface is divided into two parts, one part is the phase compensation caused by the distance from the feed to the surface, calculated by $k_0|\mathbf{r}_{mn} - \mathbf{r}_f|$, which mainly affects the focusing characteristics of the vortex electromagnetic beam; the other part is the phase compensation required for the vortex wave formed on the incident surface of the plane wave, the size of which is $l\phi_{mn}$. It mainly affects the vortex characteristic of the vortex electromagnetic beam, that is, the mode purity of the vortex wave.

Figure 2(b) is the compensation phase distribution required to generate the vortex electromagnetic wave of $l=3$ when the source wave and the plane wave are incident on the metasurface. It can be seen that the factor causing the central phase disorder is mainly due to the fact that the metasurface unit cannot be approximated as a point. Therefore, when a single unit is on the boundary line of phase change, a single unit cannot provide a variety of different phases, thereby causing phase chaos, as shown by the dotted line portion of the plane wave incident in the figure, it can be seen that if it is an ideal metasurface (if the number

of surface elements is infinite, each unit can be approximated to one point), then the phase compensation should be 0° and 180° on both sides of the dotted line, and the coded metasurface passes through some units in the dotted line, resulting in phase compensation of 0° and 180° is not possible in the same unit. This is not obvious when moving away from the center. As it gets closer to the center, the distance between the boundaries decreases, causing a unit to be crossed by multiple boundaries. Since the cause of this problem is the problem of the unit relative to the size of the metasurface, that is, the number of cells, even if the feed wave is incident, the problem still exists at the center of the metasurface, as shown in Fig. 2(b).

It can be seen from Fig. 3(a) that when the orbital angular momentum increases, the angle between the two main lobes increases. When the orbital angular momentum increases from 3 to 5, the two main lobes of the pattern (recorded as ML1) are generated. Two lower main lobes (denoted as ML2) have been analyzed and found to be vortex electromagnetic waves with an orbital angular momentum of 1. The reason is the central phase chaos, the number of elements fixed, and the orbital angular momentum increasing, the boundary line passing through the central phase unit is more, in other words, the probability of mutation is greater. As can be seen from Fig. 3(b), ML2 weakens as the surface size increases. Here, the mode purity is defined. $MP = A_{ML2} / (A_{ML1} + A_{ML2})$ represents the proportion of vortex electromagnetic waves carrying ML2 in all modes of vortex electromagnetic waves generated, A_{ML1} and A_{ML2} represent the electric field strength of ML1 and ML2, respectively. By calculation, it can be obtained that when the metasurface scale is 20×20 , that is, $M = N = 20$, $MP = 47.4\%$, when the metasurface scale is 40×40 , that is, $M = N = 40$ and $MP = 40.9\%$. As shown in Fig. 3(d),(f), the expansion of the metasurface scale increases the number of cells, and each cell is closer to a point with respect to the entire metasurface, and the increase in the total number of objects reduces the influence of phase mutations of individual cells. The influence of the central phase chaos is weakened. As shown in Fig. 3(c), the increase of k does not affect the intensity of ML2, but the phase chaos effect of the adjustment center is not obvious, but the side lobes outside the two main lobes are reduced, confirming that the k value can reduce the intensity of part of the side lobes. It can be seen from Fig. 3(d),(e) that the increase of the k value does not solve the central phase chaos problem, and it can be seen that the phase distribution of $l = 1$ appears in the central portion respectively; as can be seen from (d),(f), when the number of cells increases, the center compensation phase chaos is relatively reduced relative to the entire surface. In summary, if the performance of the vortex electromagnetic wave is to be improved, the cell size should be increased, but as the cell size increases, it is very difficult for the unit to maintain the transmission performance at a large incident angle.

In order to use the phase chaos generated by the coded metasurface center phase, this paper proposes to optimize the phase distribution using an optimization algorithm to improve the pattern.

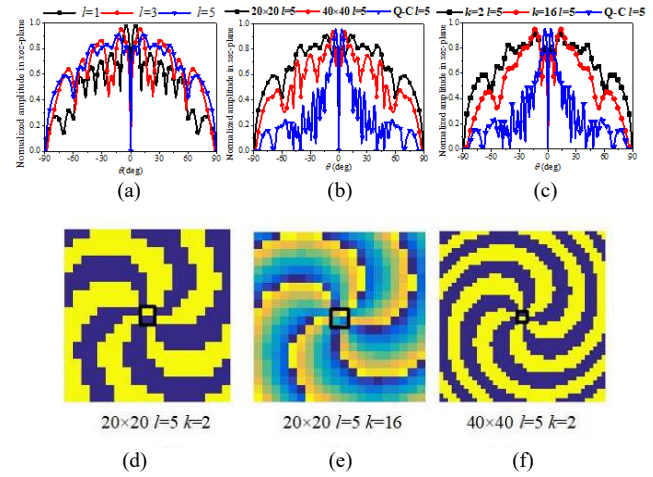


Fig. 3. The normalized radiation pattern of vortex electromagnetic wave in different parameters: (a) The normalized radiation pattern in different orbital angular momentum when the metasurface size is 20×20 and $k = 2$; (b) The normalized radiation pattern in different metasurface size when $k = 2$ and $l = 5$; (c) The phase distribution in different k when $l = 5$ and the metasurface size is 20×20 ; (d) The compensation phase when the metasurface size is 20×20 , $l = 5$ and $k = 2$; (e) The compensation phase when the metasurface size is 20×20 , $l = 5$ and $k = 16$; (f) The compensation phase when the metasurface size is 40×40 , $l = 5$ and $k = 2$.

2.2 Genetic Algorithm Optimization Principle and Unit Arrangement

Figure 4 shows a comparison of the algorithm flow chart and the unit arrangement using the algorithm to optimize the front and rear direction maps. From Fig. 4(a),(b),(c),

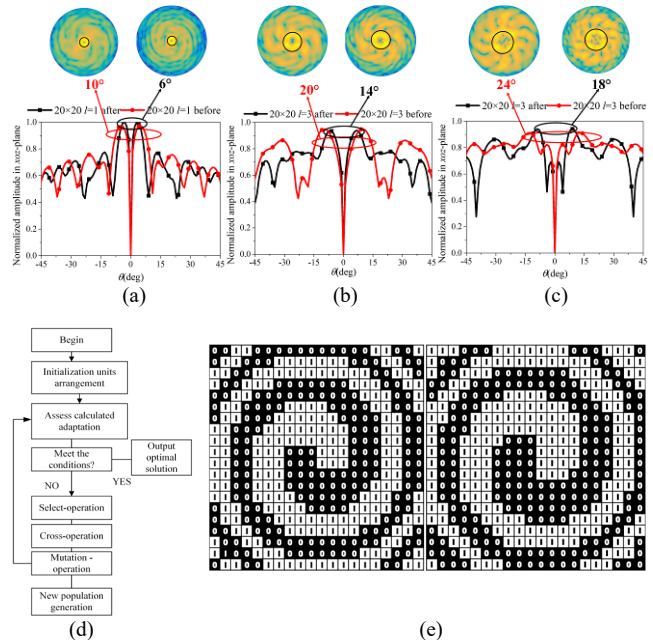


Fig. 4. (a), (b), (c) Comparison of directional diagrams before (on the left) and after (on the right) genetic algorithm optimization, and the angle between the two main lobes are labeled in different colors; (d) Genetic algorithm flowchart; (e) Comparison of unit arrangement before and after optimization.

respectively, the orbital angular momentum $l = 1, l = 2, l = 3$ are the pattern before and after the optimization unit arrangement. The angle between the two main lobes is reduced by 50%, 35%, 25%, the side lobes are significantly reduced, the energy is more concentrated on the two main lobes, and when $l = 5$ MP decreased from 47.4% to 42.4%. Figure 4(d) shows a flow chart of the genetic algorithm. Figure 4(e) shows an arrangement of two units optimized for $l = 1$, where "1" represents a unit having a transmission phase of 180° and "0" represents a unit having a transmission phase of 0° .

3. Simulation and Measured Results

In order to verify the feasibility of the method, as shown in Fig. 5, a transmissive unit with a scale of $l = 1, k = 2$ and a size of 20×20 is designed. The green rectangle is a metal patch, and the shape of the three layers of metal patches in the upper and lower layers is exactly the same. Both layers are made of Rogers RT 5880 with a dielectric constant of 2.2. LB is the length of the metal patch, L is the width of the medium, WB is the width of the metal patch, and t is the thickness of the single layer of media. A transmission phase deflection of 180° is achieved at $f = 8.8$ GHz, and the transmittance is maintained above 0.8 in the range of LB 4 to 10 mm, using discrete phase control, $LB = 4$ mm and $LB = 10$ mm with better transmittance. At two points, the transmittance reaches 0.99 or more, and the phase difference between these two points is just 174° , which is close to the phase difference of 180° . The 360° can be divided into two regions, so that the value is in accordance with (3).

$$\phi_{mn}^c = \begin{cases} 0 & \pi > \phi_{mn}^c \geq 0 \\ \pi & 2\pi > \phi_{mn}^c \geq \pi \end{cases} \quad (4)$$

Figure 6(a)–(h) shows the simulated and measured electric field complex modulus and phase distribution, respectively. It can be seen that the vortex electromagnetic wave generated after optimization features are improved and the feasibility of the proposed method is confirmed. The vortex wave energy resulting from the algorithmic optimization unit arrangement is more converged and the phase distribution is clearer.

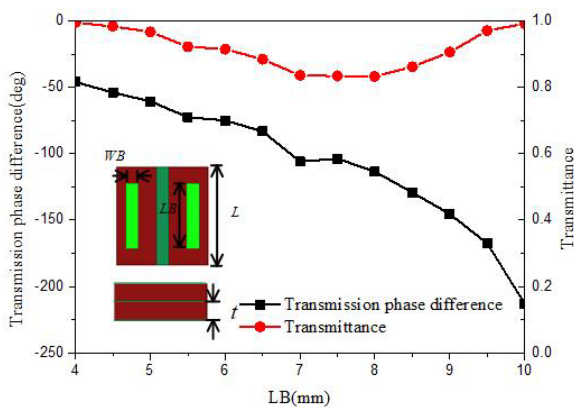


Fig. 5. Transmittance and transmission phase curves of ultra-surface units.

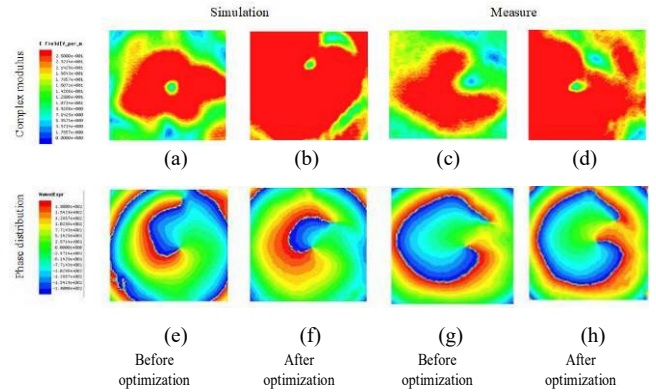


Fig. 6. Simulation results of vortex waves before and after optimization; (a),(b),(c),(d),(e),(f),(g),(h) the complex modulus and phase distribution of electric field before and after optimization in simulation and measured results, respectively.

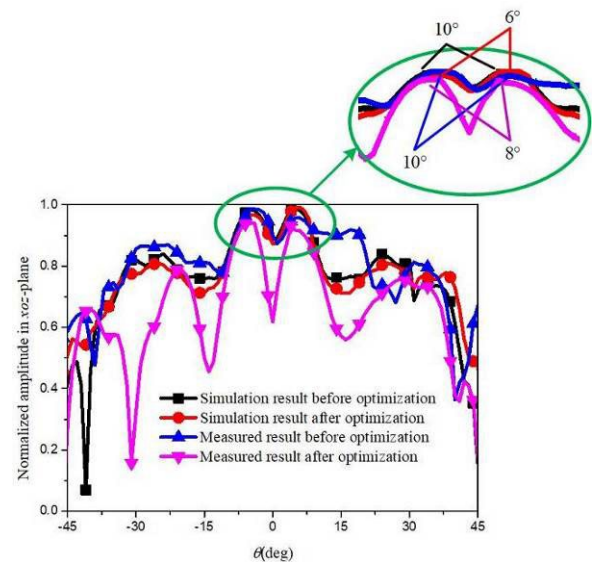


Fig. 7. The comparison between the simulation results and the measured results of the direction diagram in xoz before and after optimization.

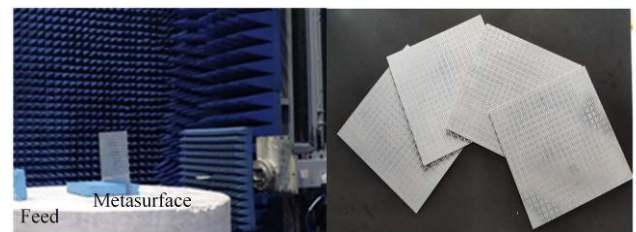


Fig. 8. The test environment and samples to be tested.

Figure 7 shows a comparison of the simulation results of the xoz plane pattern before and after optimization. It can be seen that the angle between the two main vortex waves becomes smaller and the energy is concentrated on the main lobe. It is proved that the algorithm optimizes the coded metasurface unit arrangement. It can improve the eddy wave characteristics of the metasurface.

Figure 8 shows measured environment pictures and over-surface pictures to be tested.

4. Conclusion

In this paper, the vortex wave is generated by using the coded metasurface. The simulation proves that the effect of approximating the quasi-continuous metasurface can be achieved by adjusting the phase spacing, which minimizes the difficulty of unit design. However, the simulation found that the method has certain limitations. In view of this, this paper proposes to use genetic algorithm to optimize the cell arrangement, reduce the vortex wave clutter, reduce the angle between the two main lobes, and concentrate the energy on the two main values to facilitate the propagation, which reduces the difficulty of the unit design while maintaining the quality of the vortex wave. The discrete phase elements are designed and their phase spacing is 180° . The direction diagrams before and after the algorithm optimization are compared. It is proved that the effect of the vortex wave generated by the genetic algorithm is improved. The feasibility of the method is illustrated, and the corresponding physical objects are designed and tested. The results are generally consistent.

Acknowledgments

This project is supported by the National Natural Science Foundation of China (62171460).

References

- [1] MORABITO, A. F., DI DONATO, L., ISERNIA, T. Orbital angular momentum antennas: Understanding actual possibilities through the aperture antennas theory. *IEEE Antennas and Propagation Magazine*, 2018, vol. 60, no. 2, p. 59–67. DOI: 10.1109/MAP.2018.2796445
- [2] BARBUTO, M., ALÙ, A., BILOTTI, F., et al. Dual-circularly polarized topological patch antenna with pattern diversity. *IEEE Access*, 2021, vol. 9, p. 48769–48776. DOI: 10.1109/ACCESS.2021.3068792
- [3] WANG, J., LIU, K., CHENG, Y., et al. Vortex SAR imaging method based on OAM beams design. *IEEE Sensors Journal*, 2019, vol. 19, no. 24, p. 11873–11879. DOI: 10.1109/JSEN.2019.2937976
- [4] LIU, K., LI, X., GAO, Y., et al. Microwave imaging of spinning object using orbital angular momentum. *Journal of Applied Physics*, 2017, vol. 122, p. 1–7. DOI: 10.1063/1.4991655
- [5] CHO, Y. H., BYUN, W. J. Generalized Friis transmission equation for orbital angular momentum (OAM) radios. *IEEE Transactions on Antennas and Propagation*, 2019, vol. 67, no. 4, p. 2423–2429. DOI: 10.1109/TAP.2019.2891438
- [6] QIN, H., TSO, R. Efficient quantum secret sharing based on polarization and orbital angular momentum. *Journal of the Chinese Institute of Engineers*, 2019, vol. 42, no. 2, p. 143–148. DOI: 10.1080/02533839.2018.1553634
- [7] ZHANG, Z., XIAO, S., LI, Y., et al. A circularly polarized multimode patch antenna for the generation of multiple orbital angular momentum modes. *IEEE Antennas and Wireless Propagation Letters*, 2017, vol. 16, p. 521–524. DOI: 10.1109/LAWP.2016.2586975
- [8] HU, J., BRÈS, C. S., HUANG, C. B. Talbot effect on orbital angular momentum beams: Azimuthal intensity repetition-rate multiplication. *Optics Letters*, 2018, vol. 43, no. 16, p. 4033–4036. DOI: 10.1364/OL.43.004033
- [9] ZHENG, Q., LI, Y., HAN, Y., et al. Efficient orbital angular momentum vortex beam generation by generalized coding metasurface. *Applied Physics A*, 2019, vol. 125, no. 2, p. 1–5. DOI: 10.1007/s00339-018-2373-z
- [10] ZHANG, K., YUAN, Y., ZHANG, D., et al. Phase-engineered metalenses to generate converging and non-diffractive vortex beam carrying orbital angular momentum in microwave region. *Optics Express*, 2018, vol. 26, no. 2, p. 1351–1360. DOI: 10.1364/OE.26.001351
- [11] ZHANG, Z., ZHENG, S., JIN, X., et al. Generation of plane spiral OAM waves using traveling-wave circular slot antenna. *IEEE Antennas and Wireless Propagation Letters*, 2016, vol. 16, p. 8–11. DOI: 10.1109/LAWP.2016.2552227
- [12] RUFFATO, G., ROSSI, R., MASSARI, M., et al. Design, fabrication and characterization of Computer Generated Holograms for anti-counterfeiting applications using OAM beams as light decoders. *Scientific Reports*, 2017, vol. 7, no. 1, p. 1–13. DOI: 10.1038/s41598-017-18147-7
- [13] YANG, H., YANG, F., CAO, X. Y., et al. A 1600-element dual-frequency electronically reconfigurable reflectarray at X/Ku bands. *IEEE Transactions on Antennas and Propagation*, 2017, vol. 65, no. 6, p. 3024–3032. DOI: 10.1109/TAP.2017.2694703
- [14] ZHAO, Y., GAO, J., CAO, X., et al. In-band RCS reduction of waveguide slot array using metasurface bars. *IEEE Transactions on Antennas and Propagation*, 2017, vol. 65, no. 2, p. 943–947. DOI: 10.1109/tap.2016.2633951
- [15] QIN, F., WAN, L., LI, L., et al. A transmitted metasurface for generating OAM beams. *IEEE Antennas and Wireless Propagation Letters*, 2018, vol. 17, no. 10, p. 1793–1796. DOI: 10.1109/LAWP.2018.2867045
- [16] YU, S., LI, L., KOU, N. Generation, reception and separation of mixed-state orbital angular momentum vortex beams using metasurfaces. *Optical Materials Express*, 2017, vol. 7, no. 9, p. 3312–3321. DOI: 10.1364/OME.7.003312
- [17] LI, G., KANG, M., CHEN, S., et al. Spin-enabled plasmonic metasurfaces for manipulating orbital angular momentum of light. *Nano Letters*, 2013, vol. 13, no. 9, p. 4148–4151. DOI: 10.1021/nl401734r
- [18] CHEN, C. F., KU, C. T., TAI, Y. H., et al. Creating optical near-field orbital angular momentum in a gold metasurface. *Nano Letters*, 2015, vol. 15, no. 4, p. 2746–2750. DOI: 10.1021/acs.nanolett.5b00601
- [19] XU, H. X., LIU, H., LING, X., et al. Broadband vortex beam generation using multimode Pancharatnam-Berry metasurface. *IEEE Transactions on Antennas and Propagation*, 2017, vol. 65, no. 12, p. 7378–7382. DOI: 10.1109/TAP.2017.2761548
- [20] ZHANG, D., CAO, X. Y., YANG, H., et al. Aperture efficiency and mode constituent analysis for OAM vortex beam generated by digital metasurface. *Chinese Physics B*, 2019, vol. 28, no. 3, p. 1–7. DOI: 10.1088/1674-1056/28/3/034204
- [21] ZHANG, C., CHENG, Q., YANG, J., et al. Broadband metamaterial for optical transparency and microwave absorption. *Applied Physics Letters*, 2017, vol. 110, no. 14, p. 1–5. DOI: 10.1063/1.4979543
- [22] HAN, Y., CHE, W. Q. Low-profile broadband absorbers based on capacitive surfaces. *IEEE Antennas and Wireless Propagation Letters*, 2016, vol. 16, p. 74–78. DOI: 10.1109/LAWP.2016.2556753

- [23] DING, F., CUI, Y. X., GE, X. C., et al. Ultra-broadband microwave metamaterial absorber. *Applied Physics Letters*, 2017, vol. 100, no. 10, p. 1–4. DOI: 10.1063/1.3692178
- [24] ZHANG, D., CAO, X. Y., YANG, H., et al. Multiple OAM vortex beams generation using 1-bit metasurface. *Optics Express*, 2018, vol. 26, no. 19, p. 24804–24815. DOI: 10.1364/oe.26.024804

About the Authors ...

ShiQi LV was born in Xi'an Municipality, in 1995. He received the B. Sc. degree from Xi'an JiaoTong University in 2017 and received master degree from the Air Force Engineering University in 2019. His research interest is in electromagnetic metamaterial. His research activity has been focused in the broadband and fractal artificial magnetic conductor, coding metamaterial and its application for producing vortex waves.

Xiangyu CAO received the B. Sc. and M.A. Sc. degrees from the Air Force Missile Institute in 1986 and 1989, respectively. She joined the Air Force Missile Institute in 1989 as an assistant teacher. She became an Associate Professor in 1996. She received Ph.D. degree in the Missile Institute of Air Force Engineering University in 1999. From 1999 to 2002, she was engaged in postdoctoral research in Xidian University, China. She was a Senior Research Associate in the Dept. of Electronic Engineering, City University of Hong Kong from June 2002 to Dec 2003. She is currently a Professor of Information and Navigation College of the Air Force Engineering University of

CPLA. She is the IEEE senior member from 2008. She has authored and coauthored more than 200 technical journal articles and conference papers, and holds one China soft patent. She is the coauthor of two books entitled, *Electromagnetic Field and Electromagnetic Wave*, and *Microwave Technology and Antenna* published in 2007 and 2008, respectively. Her research interests include smart antennas, electromagnetic metamaterial and their antenna applications, and electromagnetic compatibility. She is a reviewer of *Applied Physics Letter*, *Journal of Applied Physics*, *IEEE Transactions on Antennas & Propagation*, and *IEEE Antennas Wireless Propagation Letter*.

Jun GAO received the B. Sc. and M.A. Sc. degrees from the Air Force Missile Institute in 1984 and 1987, respectively. He joined the Air Force Missile Institute in 1987 as an assistant teacher. He became an Associate Professor in 2000. He is currently a Professor of Information and Navigation College, Air Force Engineering University of CPLA. He has authored and coauthored more than 100 technical journal articles and conference papers, and holds one China soft patent. His research interests include smart antennas, electromagnetic metamaterial and their antenna applications.

RongZhen XUE was born in Xi'an Municipality, in 1987. He received the B. S. degree from Xidian University in 2010. His research interest is in electromagnetic metamaterial. His research activity has been focused in the antenna array design, electromagnetic field numerical calculation.